

## Cosmic-ray energetics and mass (CREAM) balloon project

E.S. Seo <sup>a,\*</sup>, H.S. Ahn <sup>a</sup>, J.J. Beatty <sup>b</sup>, S. Coutu <sup>b</sup>, M.J. Choi <sup>c</sup>, M.A. DuVernois <sup>d</sup>,  
O. Ganel <sup>a</sup>, T.G. Kang <sup>a</sup>, K.C. Kim <sup>a</sup>, M.H. Lee <sup>a</sup>, L. Lutz <sup>a</sup>, P.S. Marrocchesi <sup>e</sup>,  
S. Minnick <sup>b</sup>, K.W. Min <sup>f</sup>, S. Nutter <sup>g</sup>, H. Park <sup>h</sup>, I.H. Park <sup>c</sup>, E. Schindhelm <sup>a</sup>,  
R. Sina <sup>a</sup>, S. Swordy <sup>i</sup>, J. Wu <sup>a</sup>, J. Yang <sup>c</sup>

<sup>a</sup> Institute for Physical Science and Technology, University of Maryland, College Park, MD 20742-2431, USA

<sup>b</sup> Department of Physics, Penn State, University Park, PA 16802, USA

<sup>c</sup> Department of Physics, Ewha Woman's University, Seoul 120-750, South Korea

<sup>d</sup> School of Physics and Astronomy, University of Minnesota, Minneapolis, MN 55455, USA

<sup>e</sup> Department of Physics, University of Siena, and INFN, Siena 53100, Italy

<sup>f</sup> Department of Physics, Korea Advanced Institute of Science and Technology, Taejeon 305-701, South Korea

<sup>g</sup> Department of Physics and Geology, Northern Kentucky University, Highland Heights, KY 41099, USA

<sup>h</sup> Department of Physics, Kyungpook National University, Taegu 702-701, South Korea

<sup>i</sup> Enrico Fermi Institute and Department of Physics, University of Chicago, Chicago, IL 60637, USA

Received 22 November 2002; received in revised form 25 April 2003; accepted 2 May 2003

### Abstract

The cosmic-ray energetics and mass (CREAM) investigation is designed to measure cosmic-ray composition to the supernova energy scale of  $10^{15}$  eV in a series of ultra long duration balloon (ULDB) flights. The first flight is planned to be launched from Antarctica in December 2004. The goal is to observe cosmic-ray spectral features and/or abundance changes that might signify a limit to supernova acceleration. The particle charge ( $Z$ ) measurements will be made with a timing-based charge detector and a pixelated silicon charge detector to minimize the effect of backscatter from the calorimeter. The particle energy measurements will be made with a transition radiation detector (TRD) for  $Z > 3$  and a sampling tungsten/scintillator calorimeter for  $Z \geq 1$  particles, allowing inflight cross calibration of the two detectors. The status of the payload construction and flight preparation are reported in this paper.

© 2004 COSPAR. Published by Elsevier Ltd. All rights reserved.

**Keywords:** Scientific balloon payloads; CREAM; Cosmic-ray measurements; Particle detectors

### 1. Introduction

Cosmic rays were discovered by Victor Hess in 1912 using a balloon-borne pressurized ionization chamber. Elementary particles were discovered in cosmic rays, and their properties were known qualitatively before man-made accelerators became available to study the details of particle properties and nuclear interactions. The cosmic rays are comprised of essentially all the elements in the periodic table. With notable exceptions,

their composition is similar to that measured in the solar system. The cosmic-ray flux decreases rapidly as energy increases, and the energy spectrum follows a power law that is characteristic of shock acceleration. At low energies, where the flux is high, cosmic rays have become relatively well understood in the intervening  $\sim 90$  years to result from energetic processes in the galaxy, probably from supernova explosions. However, the origin of high-energy cosmic rays is still a mystery because their energies extend several orders of magnitude beyond the limit thought possible for supernova shock waves. The cosmic-ray spectral features known as the “knee” and the “ankle” are believed to reflect changes in sources, propagation, and/or acceleration. The “knee” is a

\* Corresponding author. Tel.: +1-301-405-4855; fax: +1-301-314-9363.

E-mail address: [seo@umd.edu](mailto:seo@umd.edu) (E.S. Seo).

transition region where the all-particle spectrum steepens from  $dN/dE \sim E^{-2.7}$  below  $10^{14}$  eV to  $\sim E^{-3.3}$  above  $10^{16}$  eV, and the “ankle” is where the spectrum flattens back to  $\sim E^{-2.7}$  at  $\sim 10^{19}$  eV.

Cosmic rays in the energy range  $10^{14}$ – $10^{20}$  eV have been detected in ground-based observations of air showers in the atmosphere. The weakness of such indirect measurements is that the primary particle that initiated the air shower cannot be identified. On the other hand, cosmic rays can be measured directly by flying particle detectors on spacecraft or high altitude balloons. In the latter case, the primary particle identity and its energy can be determined unambiguously, but the energy reach is limited by the detector size and exposure time.

Energy spectra of primary cosmic rays are known with good precision up to energies around  $10^{11}$  eV, where magnetic spectrometers have been measuring spectra. Above this energy the composition and energy spectra are not accurately known although there have been some pioneering measurements (Müller et al., 1991; Asakimori et al., 1998; Apanasenko et al., 1999). For example, Asakimori et al. (1998) have reported a difference in the spectral indices for Hydrogen and Helium, but Apanasenko et al. (1999) do not see such a difference. By taking all existing data at face value, some unexpected behaviors are found. As shown in Fig. 1, the flux of helium relative to protons appears to increase with energy. This behavior could be interpreted as

evidence for two different types of sources/acceleration mechanisms for H and He (Biermann, 1993). A bend in the proton spectrum has been reported previously to occur near 2 TeV (Grigorov et al., 1971), whereas a different study indicated a bend around 40 TeV (Asakimori et al., 1993). These roll-off energies for protons are one to two orders of magnitude below the “knee” seen in the all-particle spectrum. There seems to be also an overall trend for the spectra of heavier elements to become flatter with increasing energy. Specifically, the spectral slopes at higher energies seem to be close to values around 2.5–2.6 which is significantly flatter than the low energy slopes.

Cosmic-ray propagation at high energies is dominated by escape from the galaxy, which is dependent on particle rigidity ( $R$ ). From measurements of secondary cosmic rays generated by spallation of primary nuclei in the interstellar medium (ISM), the mean escape length,  $\lambda_e$ , is known to decrease with increasing energy up to  $\sim 100$  GeV/nucleon, specifically  $\lambda_e \propto R^{-\delta}$  where  $\delta \sim 0.6$ . The flattening of all heavier nuclei spectra could be explained by a less severe decline in the escape length above 1 TeV/nucleon, i.e. with  $\delta < 0.6$ . The absence of data on the relative abundance of secondary cosmic rays above  $\sim 10^{12}$  eV/nucleon makes it difficult to deduce the galactic propagation history of cosmic rays, so the energy spectrum observed near Earth cannot be related to the spectrum with which the particles must be accelerated at the source. Measurements of the detailed energy dependence of the elemental spectra to as high an energy as possible is key to understanding the acceleration and galactic propagation for the bulk of cosmic rays, i.e. those at energies below the knee in the all-particle spectrum.

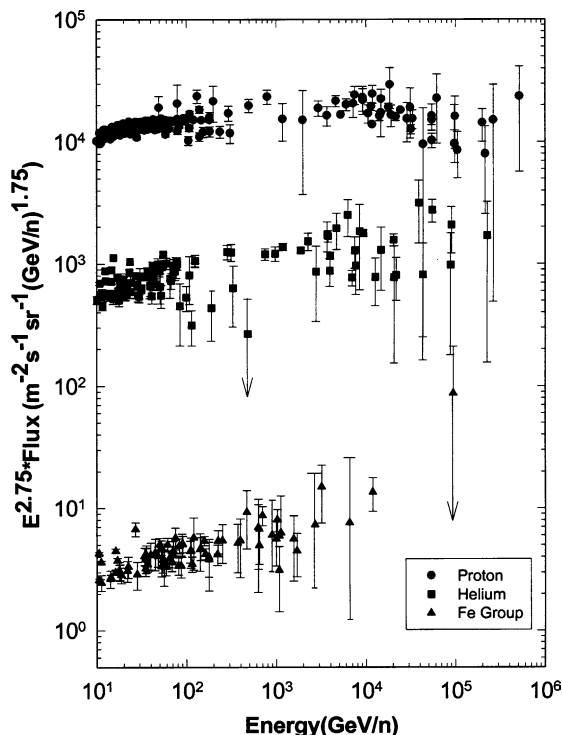


Fig. 1. Compiled data from direct measurements.

## 2. Shock acceleration

Theories of diffusive shock acceleration have shown that the resulting energy spectrum follows a characteristic power law. Shock waves and the associated power law spectra are observed within the heliosphere, and they are believed to be prevalent in astrophysical plasmas at all scales throughout the Universe. Particles pick up a small increment of energy each time they cross a shock in a diffusive process, analogous to a pingpong ball getting accelerated between two moving ping pong paddles. Supernovae are good candidates for the cosmic-ray source, because shock acceleration by supernova blast waves can produce power law energy spectra, and their power and frequency can explain the average energy density of cosmic rays in the Universe. Recent observations of non-thermal X-ray spectra (Koyama et al., 1995) provide compelling evidence that supernova remnants are acceleration sites of electrons. However, it

is difficult to infer hadron acceleration in supernovae from these data.

The maximum particle energy ( $E_{\max}$ ) that can be achieved from shock acceleration depends on the magnetic field ( $B$ ) associated with the shock and on the time ( $T$ ) taken for the shock wave to propagate outward and weaken to the point that it is no longer an efficient mechanism:

$$E_{\max} \sim \frac{v}{c} ZeBVT,$$

where  $Z$  is the particle charge (atomic number) and  $V$  is the shock expansion speed. The nominal energy limit  $E_{\max}$  is about  $Z \times 10^{14}$  eV (Lagage and Cesarsky, 1983), with nominal values of  $B \sim 3 \mu\text{G}$ ,  $T \sim 1000$  years and  $V \sim 5000$  km/s. Protons should be most abundant at low energies but heavier elements should become more abundant above the proton acceleration limit  $\sim 10^{14}$  eV and eventually iron should become most abundant  $> 10^{15}$  eV. The corresponding iron nuclei limit ( $\sim 26 \times 10^{14}$  eV) is nowhere near the observed maximum cosmic-ray energy ( $\sim 10^{20}$  eV) but it is intriguingly close to the “knee” feature observed by many air shower experiments around  $3 \times 10^{15}$  eV. A characteristic change in the cosmic-ray elemental composition between the limiting energies for protons and iron would be the signature of the supernova acceleration limit, thereby connecting the origin of cosmic rays to supernova blast waves.

### 3. Science goals

The following key scientific questions will be addressed by CREAM: (1) Are supernovae really the sources of cosmic rays? (2) What is the history of cosmic rays in the Galaxy? (3) Can the energy spectrum of cosmic rays result from a single mechanism? (4) What is the origin of the “knee” of the cosmic-ray energy spectrum? To answer these questions CREAM must (1) determine whether or not the spectral slopes of the heavier nuclei are the same as that of helium and different from that of protons; (2) measure the potential changes in the spectra of secondary nuclei; and (3) search for spectral features such as a bend in the proton spectrum. CREAM will study the composition change by measuring the energy spectra from  $10^{12}$  to  $10^{15}$  eV over the elemental range from protons to iron. These high-energy composition measurements are difficult because of the very low particle fluxes. The detectors must be large enough to collect adequate statistics, yet stay within the weight limit for space flight. Innovative detector systems coupled with the ultra long duration balloon (ULDB) capability being developed by NASA now promise high quality measurements over an energy range that was not previously possible.

### 4. Instrument

Our cosmic-ray energetics and mass (CREAM) instrument must determine the charge  $Z$  and energy  $E$  of the incoming particles to meet the measurement objectives. As shown schematically in Fig. 2, a variety of particle detectors are used for these measurements. The particle charge is measured with the timing charge detector (TCD), silicon charge detector (SCD), and S0/S1 scintillating fiber hodoscopes. The key design consideration for charge measurements is to minimize the effects of backplash particles from the showers produced in the calorimeter. This is accomplished either by detector segmentation or by a timing technique. A finely segmented silicon charge detector has been flown on the advanced thin ionization calorimeter – ATIC (Wefel et al., 2001), and a similar technique is employed for the CREAM SCD. Four layers of scintillating fibers, S0/S1, provide additional charge measurements as well as particle tracking information. The timing technique is a new technology being developed for CREAM (Beatty et al., 1999).

The particle energy is measured with a transition radiation detector (TRD) and an ionization calorimeter. For particles with  $Z > 3$  the TRD measures a signal

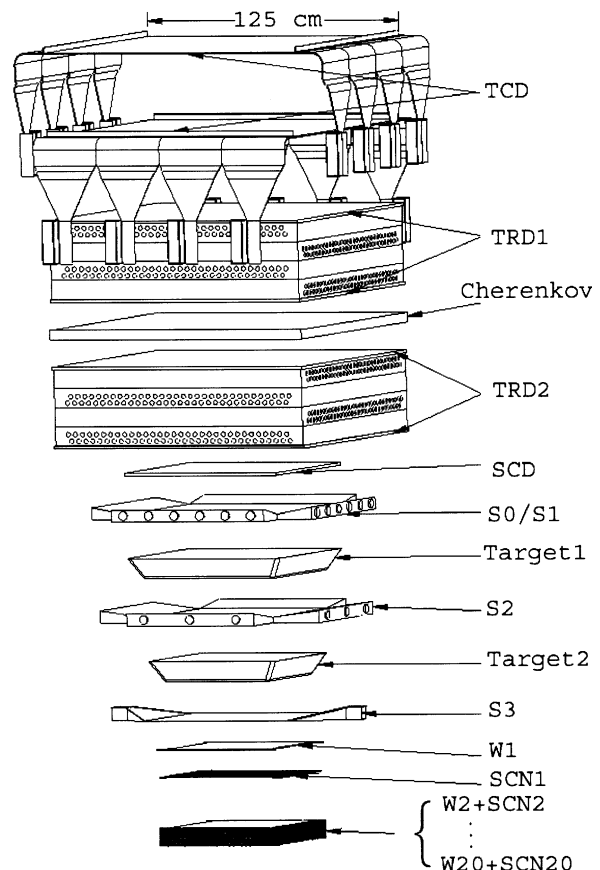


Fig. 2. Schematic of the CREAM instrument configuration.

which is a function of the charge and the Lorentz factor  $\gamma$ . The TRD is divided into two sections separated by a plastic Cherenkov detector. The Cherenkov detector responds only to particles with velocity exceeding the velocity of light in the plastic, so it allows rejection of the abundant low energy cosmic rays present in the high latitude regions where the geomagnetic cutoff is low.

Ionization calorimetry provides the only practical method for measuring the energy of protons and helium up to the energies of interest to CREAM. The measurement is based on the principle that a particle's energy is deposited inside an absorber via a cascade of nuclear and electromagnetic interactions. At each step of the cascade the energy of the primary particle is subdivided among many secondary particles. Ultimately, the primary energy of an incident hadron is dissipated via ionization and excitation of the absorbing material. This cascade is much like a compressed air shower generated by high energy cosmic rays entering the Earth's atmosphere.

CREAM employs a tungsten-scintillator sampling calorimeter preceded by a carbon target. It can determine the particle's energy for all nuclei including particles with  $Z < 3$  for which the TRD cannot reliably provide an indication of the particle energy. The TRD and calorimeter have different systematic biases in determining the particle energy. The use of both instruments allows in-flight intercalibration of the two techniques and thus a more reliable energy determination. While both detector types have been flown separately in prior balloon investigations, the CREAM instrument is the first balloon payload to employ a calorimeter and TRD together for high energy composition measurements.

#### 4.1. Timing charge detector

The timing charge detector (TCD), which fully covers the top of the instrument, provides charge measurements for particles that enter the TRD acceptance. It consists of two layers of four plastic scintillator paddles. Each scintillator paddle is 120 cm long, 30 cm wide, and 0.5 cm thick. On both ends, each paddle has adiabatic clear plastic light guides that are mated to fast photomultiplier tubes (PMT) having two readouts.

For events with a shower in the calorimeter, about 75 cm below the TCD, one expects back-scattered shower secondaries to traverse the scintillator paddles several nanoseconds after the primary has gone through. This back ground noise is nearly proportional to the logarithm of the incident particle energy. The charge signal can be separated from the back-scattered background by taking advantage of the brief time interval between the primary signal and the back-scatter noise. The first readout is based on 10 comparators, with multiple TDCs digitizing the time at which the leading edge of

the scintillation light pulse crosses the thresholds. From the timing signals the TCD data processing code will reconstruct the slope of the pulse's leading edge, which is proportional to the square of the incident particle charge. Some scintillation saturation is expected for charges between about 5 and 14, but this can be reconstructed in the offline analysis. The second readout captures the peak level and digitizes it using an ADC. This too is proportional to the square of the incident charge. The first readout is expected to be more accurate for lower charges (up to  $Z = 15$ ), while the second is expected to be more accurate for higher charges where back-scatter has a much lower impact.

The so-called S3 detector provides a reference time for the TCD. Located just above the calorimeter stack, it is a single layer of  $2 \times 2$  mm<sup>2</sup> square, multi-clad scintillating fibers. The fibers are all collected into a roughly circular array on either end, where a Lucite cylinder is glued onto the fiber faces. The other ends of these light mixers are mated to the same type of PMT and readouts as described above. For events with a shower in the calorimeter the shower secondaries traversing S3 generate a fairly large signal (>100 photoelectrons for 1 TeV incident energy) in each of the two PMTs. The TDC digitizes the time at which the signal arrives on either end of S3. From this time the TCD code will reconstruct the time at which the primary (or the shower) traversed S3, and from that, by simple extrapolation, the time at which the primary traversed the upper TCD layers. This extrapolated time facilitates separation of the primary TCD signal from the back-scatter noise in those events where the geometry of the event makes such separation based on signals from the upper paddles by themselves more difficult. See Beatty et al. (1999, 2002) for TCD details.

#### 4.2. Transition radiation detector

The TRD is comprised of two modules, each with a  $120 \times 120 \times 35$  cm<sup>3</sup> active volume. Each module is comprised of eight layers (two in X orientation, two Y, two more X and two more Y) of 32 thin-walled aluminized Mylar tubes embedded in a plastic foam matrix. This matrix serves the dual purpose of radiator and mechanical support. The 512 tubes are filled with a mixture of Xenon (95%) and Methane (5%), with a signal wire strung between the two end-caps kept at 1.5 kV with respect to the grounded tube wall. The end-caps have been specially designed to minimize gas leaks to a level comparable to the leak rate through the Mylar walls. The TR signal generates charge pulses in the wires which are read out using Amplex 1.5 application specific integrated circuits (ASICs), with a high-gain and a low-gain range to cover the 12-bit dynamic range required to measure particles from Lithium to Nickel. The radiator

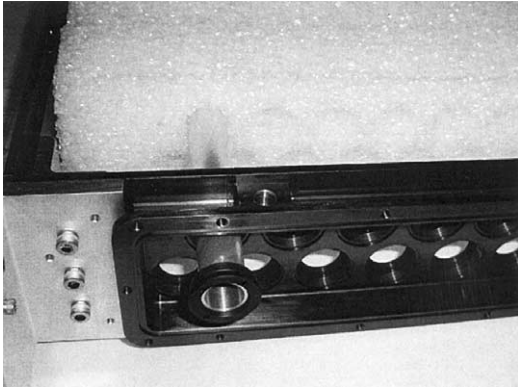


Fig. 3. Detector tube in assembly with foam regenerator and gas exit manifold.

is optimized to cover the range  $10^3 < \gamma < 10^5$ . To reject low-energy particles for data collected near the South Pole (lower geo-magnetic cutoff) a plastic Cherenkov layer has been added between the two TRD modules. This layer is divided into four quadrants, each read out using two wavelength shifting (WLS) bars with a 0.5 in. PMT at their ends. With these signals the primary can be required to be relativistic, reducing the trigger rate for non-showering events to an acceptable level between 100 and 130 Hz. Based on results from a CERN beam test in 2001, Ethafoam was chosen as the TRD radiator (see Fig. 3).

#### 4.3. Silicon charge detectors

The silicon charge detector (SCD) allows measurements of particles incident both outside and inside the TCD acceptance by fully covering the top area of the carbon target, thereby defining the acceptance of the calorimeter. The SCD is not far enough above the tungsten stack of the calorimeter to allow timing-based discrimination. Instead, it is segmented into pixels each about  $2.4 \text{ cm}^2$  in area, so back-scatter is expected to cause charge mis-identification of only about 2–3% of low- $Z$  particles near  $10^{15} \text{ eV}$  incident energy, with significantly less misidentification for lower energies and/or higher charge. The SCD active area is  $79 \times 79 \text{ cm}^2$ , with a sensor thickness of  $380 \mu\text{m}$ , and a total detector thickness of 13 mm. The sensor is designed to be modular: each module consists of 16 pixels and the readout electronics (including a 16-channel Amplex CR-1.4 ASIC) under the wafer. A sensor module is shown in Fig. 4. Kapton cables carry the analog signals multiplexed from the ASICs to two opposite sides of the SCD, outside of the active area, where they are digitized using 14-bit ADCs. One ladder of six sensor modules was tested with fragments of the Pb beam in the CERN H8 beam line in October 2002.

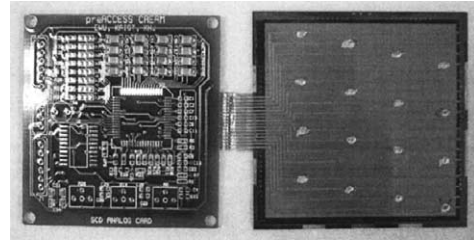


Fig. 4. Photograph of a silicon sensor module ( $4 \times 4$  pixels) with front end electronics.

#### 4.4. Fiber hodoscopes

There are three hodoscopes in the CREAM instrument. Above the graphite target layers there is a pair of hodoscopes with a total of four crossed layers of  $2 \times 2 \text{ mm}^2$  square fibers. The upper hodoscope, S0 is comprised of scintillating fibers aluminized on one end near the edge of the active area, with the other end extending outside the active area and populated into a cookie mated against a 73-pixel hybrid photo-diode (HPD). Alternate fibers are read out from opposite ends for mechanical convenience. Each layer is comprised of 360 tight-packed fibers, covering an active area of about  $79 \times 79 \text{ cm}^2$ . The lower hodoscope S1 is identical to S0 in all respects, except that the readout end of each scintillator fiber ends at the other end of the active area, where a clear fiber with identical cross-section is glued to the scintillating fiber. The clear fibers are then populated in the same cookies as the S0 scintillating fibers. Each cookie is populated with 30 S0 fibers 30 S1 fibers and four bundles of clear fibers leading to light emitting diodes (LEDs). The LEDs serve the dual purpose of cookie alignment during assembly and as the in-flight calibration light source. The third hodoscope, S2, is located between the two graphite targets. This detector is constructed in a manner similar to S1 but with shorter scintillating fibers (the active area is only  $63 \times 63 \text{ cm}^2$ ). The S2 clear fibers are populated into 12 cookies (three per side), with three clear fiber bundles allowing LED light to be inserted into pixels of the S2 HPDs. All three hodoscopes will allow improved track reconstruction, with fitting points relatively far above the thin calorimeter, thereby improving the lever arm for track fitting. The S0 and S1 hodoscopes are also expected to provide some charge reconstruction information to supplement the TCD and SCD data.

#### 4.5. Calorimeter

The calorimeter is comprised of a stack of 20 tungsten sheets, each  $50 \times 50 \times 0.35 \text{ cm}^3$ , with tabs at each corner to allow mechanical mounting onto the honeycomb pallet that acts as the base of the support structure. Each plate is approximately one radiation length in thickness,

for a total of 20 radiation lengths. A layer of fifty 10 mm wide, 500 mm long, and 0.5 mm thick scintillating fiber ribbons is mounted on top of all but the top tungsten layer. Under the bottom tungsten plate is a similarly shaped aluminum plate to allow easy mounting for the 20th scintillation layer. Each fiber ribbon is aluminized on one end and glued into an approximately adiabatic Acrylic light mixer on the readout end. The fibers are mounted with their readouts on alternating ends. Each light mixer has a bundle of 48 thin clear fibers with a black polyethylene jacket glued into its other end.

The bundle of clear fibers carries the scintillation light signal to 73-pixel HPDs identical to those used to read out the hodoscopes. Each bundle is split into three sub-bundles to create low-, mid-, and high-energy readouts. Using neutral density filters, these ranges are arranged with a relative signal strength ratio of about 30 from low- to mid-range, and another factor of 30 from mid- to high-range. The HPD dynamic range of about 1,000,000:1 is enough to easily cover the 200,000:1 required for the CREAM design goal of reconstructing energies and tracks from  $10^{12}$  to  $10^{15}$  eV. However, the IDEAS VA32HDR2 ASICs used to read out the HPDs have a dynamic range of just under 11 bits. With the 3-range readout this range is extended above the requirement, even taking into account a S/N ratio of four at the low end. Overlaps between the ranges will allow inter-range calibration with shower data. The layers are read out in alternating X and Y orientation to permit X–Z and Y–Z track reconstruction. Each layer is read out from two opposite ends, with 25 ribbons read out from one side, and the remaining 25 from the other. Each layer has 25 low-range readouts, 25 mid-range readouts, and five high-range readouts with light collected from five out of 10 neighboring ribbons. A single HPD, with two 32 channel ASICs reads out the 55 signals, as well as three LED signals. Six more pixels are read out with no light source, thereby providing a good handle on collective electronic behavior (pedestal drift, gain drift, etc.) for offline calibration. Nine of the 73 pixels are not read out at all. Five HPDs are powered by a single 12 kV HV power supply and read out with the same motherboard. Two motherboards in the same readout box are used to read out the 10 HPDs that read out one calorimeter side. Four such boxes are used to read out the entire calorimeter. The expected resolution of the calorimeter is better than 45%, with no non-Gaussian high-end tails.

After a successful beam test at CERN in September 2001 proved that the detector concept and readout design would work as expected, the components required to assemble a full calorimeter were produced. The fully populated flight calorimeter with the S2 hodoscope and S3 layer were shipped to CERN for calibration in July 2002. Fig. 5 shows the calorimeter module tested at CERN. As in the 2001 beam test, the flight targets were used. All boxes and detector components were mounted

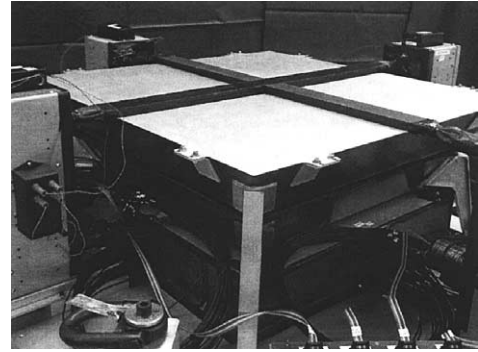


Fig. 5. Photograph of the calorimeter module including hodoscopes, carbon targets and W-scintillating fiber stack.

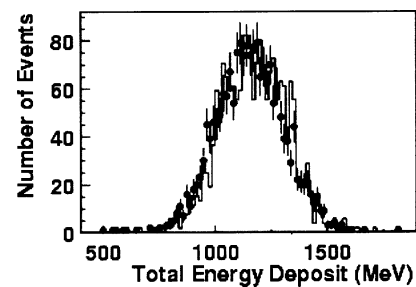


Fig. 6. Energy deposit distribution for 250 GeV electrons. The symbols represent the measurements from the beam test and the solid line represents the simulations.

to the flight aluminum honeycomb pallet which was supported by a custom rotational fixture. Online monitoring showed a clear shower-axis for 150–250 GeV electrons, as well as for 350 GeV protons. As shown in Fig. 6, the preliminary beam test result shows 250 GeV electron energy resolution ( $\sigma$ ) of  $\sim 12\%$ , which is consistent with Monte Carlo simulations. A preliminary result of the S3 test showed that the number of photoelectrons produced in shower events significantly exceeds the minimal requirement for the TCD reference time. The CREAM data processing system (CDPS), closely modeled after the ATIC ADPS system, has been completed and is in use for data calibration processing and analysis.

## 5. Ballooncraft

The term ballooncraft is used to designate all hardware below the attachment point to the mobile launch vehicle. This, with the exception of a rotator, is an integrated assembly of the instrument and support systems mounted on the primary support structure. As shown in Fig. 7, the ballooncraft consists of the ballooncraft support system and the instrument package. The ballooncraft support system has the capability to provide global coverage of telemetry downlinks and

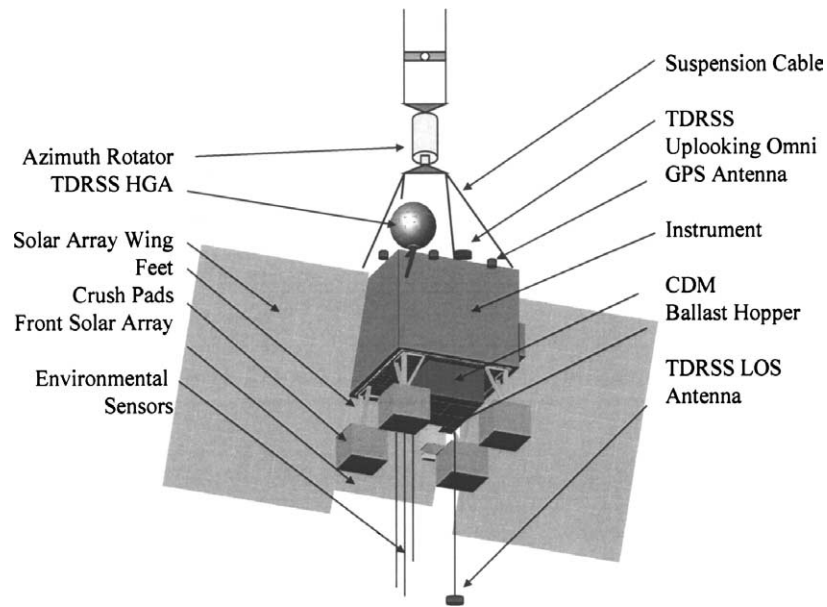


Fig. 7. CREAM ballooncraft configuration.

command uplinks, power, and data processing for the science instrument packages. It consists of the command data module (CDM), instrument support structure (ISS), Solar Array panel support system, antenna support systems, ballast hopper, and crush pads. It also monitors the health and well being of the balloon vehicle and the ballooncraft. The CDM is the core of the ballooncraft support system. It controls and monitors the ballooncraft power system and communications through a flight computer subsystem. It also controls and monitors the health and safety of the overall balloon system, stores data, and provides balloon position data. The CDM is located in an independent thermally controlled support structure. All flight systems are designed for mission duration of at least 100 days. The superpressure balloon vehicle made with a non-extensible material is a closed system to prevent gas release.

### 5.1. Mechanical system

The ISS provides the primary mechanical support for both the instrument and the ballooncraft support system. The balloon vehicle design requires that the total suspended weight not exceed 5500 lb excluding ballast. The weight breakdown, including contingency, is shown in Table 1. The mechanical structure and associated hardware are designed and built to meet the strength requirements mandated by the National Scientific Balloon Facility (NSBF). The ballooncraft is designed to survive a nominal ground impact. It is recognized, however, that some structurally mounted hardware such as the solar array and TDRSS antenna, may not survive a nominal impact. The parachute will be able to automatically separate from the ballooncraft upon ground

Table 1  
Payload weight summary

Subsystems	Weight (lb)
Instrument	2414
Flight control & flight train	941
Ballooncraft support system	2145
Ballast	750
CREAM total	6250

impact. The ballooncraft is designed such that all instrument electronics boxes, calorimeter, carbon blocks, TRDs, hard drives and TDRSS transponder can be removed with minimal tools during recovery.

### 5.2. Data system

The CREAM block diagram in Fig. 8 shows the interface between the science instrument and the ballooncraft support system. The command and data path to the ballooncraft flight computer is changed from MIL-1553B (Seo et al., 2002) to Ethernet. The nominal telemetry rates are expected to be 50 kbp for science data and <500 bp for monitoring data for support and flight control systems. The primary communications link for the mission data will be through the Tracking and Data Relay Satellite System (TDRSS). A test flight of the ballooncraft support system in early 2001 showed that the TDRSS high gain antenna (HGA) performance exceeded the requirements by transmitting data at rates up to 150 kbp. All data will also be stored on-board. All monitored and science data will be transmitted from the balloon to the Operations Control Center (OCC) at the NSBF in Palestine, Texas. The Science Team will have command and data capability from their home

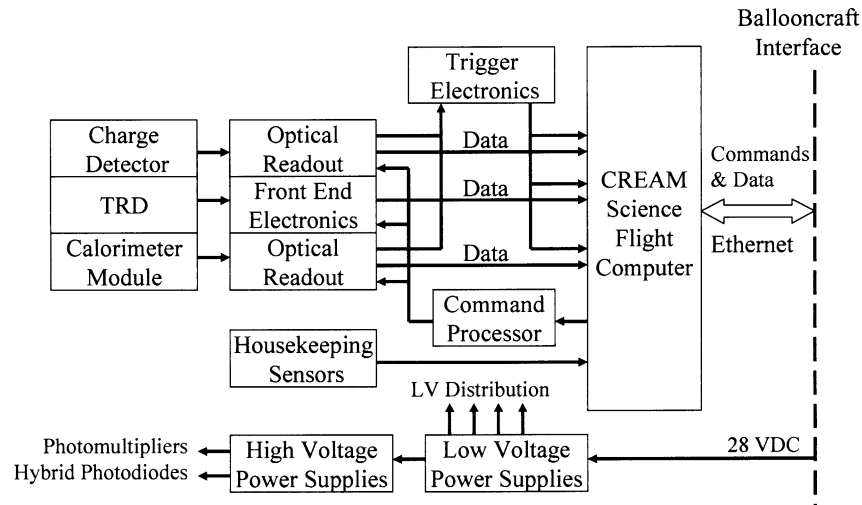


Fig. 8. CREAM block diagram.

Table 2  
Payload power summary

Subsystems	Weight (lb)
Instrument	380 W
Ballooncraft support system	170 W
CREAM total	550 W

institutions via network connections. For more details on the ballooncraft support system development status and test results see Stuchlik et al. (2004).

### 5.3. Electrical power system

The electrical power system includes a solar array for electrical power generation and batteries for energy storage. The power system must provide sufficient power to support a nominal 100-day mission with 100% duty cycle. The power system is sized for nominal flight operations within the range of 90° south latitude to 30° south latitude. The nominal operating output voltage of the power system is  $28 \pm 4$  Vdc, and the instrument is expected to draw 380 W from the primary 28 V supply. See Table 2 for the power breakdown.

## 6. Integration and test plan

The CREAM payload will float at an altitude above 110,000 ft for a period of 60–100 days. At this altitude, near-vacuum conditions cause coronal discharges between unshielded points with a potential difference as low as 100 V. The payload must also be able to survive a wide range of thermal environments. The first flight is planned for launch from Antarctica where the 24 h daylight and high albedo from the ice will increase the payload temperature. The payload may also spend considerable time at near equatorial latitudes where an

eclipse of 11 h will make the payload cold. Thermal and vacuum testing is required to verify that the payload can survive such environmental extremes (Ganel et al., 2001). The instrument verification process with component/box level vacuum tests is scheduled for completion by October 2003. The instrument subsystems will be delivered to the University of Maryland for instrument integration mid-November 2003. Mechanical and electrical integration of all the instrument subsystems including the trigger and DAQ will be completed by mid-February to have a thermal vacuum test at the end of February 2004. The instrument will be delivered to the NASA Wallops Flight Facility for integration with the ballooncraft support system in March 2004 in order to complete the ballooncraft end-to-end hang test by early June 2004. After completion of the flight system end-to-end test the payload will be shipped to Antarctica in mid-August, 2004 to be flight ready for the first launch opportunity in December, 2004.

## 7. Summary

A calorimeter and a TRD have been flown individually on a balloon, i.e., ATIC (Wefel et al., 2001) and TRACER (Gahbauer et al., 1999), but CREAM is the first instrument to have both detectors in the same payload for high-energy (>TeV) cosmic-ray composition measurements. This allows inflight cross calibration of the two techniques and, therefore, better energy determination. The CREAM TRD will measure  $Z > 3$  particles with energy resolution of  $\sim 15\%$  for carbon and  $\sim 7\%$  for iron at a Lorentz factor  $\gamma = 3000$ . The CREAM calorimeter will measure all elements including  $Z = 1$  and 2 particles with energy resolution better than 45% for all energies. The geometry factor of the TRD is  $1.3 \text{ m}^2 \text{ sr}$ , and the effective geometry of the calorimeter taking into account the in-

teraction fraction, is about  $0.3 \text{ m}^2 \text{ sr}$  for protons and respectively higher for heavier nuclei. The collecting power of CREAM is about a factor of two larger than that of ATIC for protons and, considering the larger geometry factor of the TRD, about a factor of 10 larger for heavy nuclei. The instrument has been tested and calibrated with a series of beam tests at CERN, specifically September 2001, July 2002, and October 2002. Its performance is consistent with the Monte Carlo simulations. The instrument calibration is discussed in more detail in Ganel et al. (2002). The expected instrument performance, including trigger and data rates, energy resolution, energy response, etc. is presented in Ahn et al. (2001).

The CREAM ballooncraft is designed and being constructed for a mission duration of at least 100 days to utilize the new ULDB flight capability which is being developed by NASA to achieve 60–100 days of exposure per flight. The function and reliability of the ballooncraft is to be verified and validated by integration and test prior to shipment for launch.

### Acknowledgements

This work is supported by NASA grants NAG5-5248, NAG5-5249 and NAG5-5250 in the US, by the Korean Ministry of Science and Technology in Korea, and by INFN in Italy. The authors thank the WFF team for the ballooncraft support system development.

### References

- Ahn, H.S., Beach, S., Beatty, J.J., et al. Cosmic ray energetics and mass: expected performance, in: Proc. 27th Int. Cosmic Ray Conf., Hamburg, vol. 6, pp. 2159–2162, 2001.
- Apanasenko, A.V., Beresovskaya, V.A., Fujiet, M., et al. Primary cosmic ray spectra observed by RUNJOB, The RUNJOB collaboration, in: Proc. 26th Int. Cosmic Ray Conf., Salt Lake City, vol. 3, pp. 163–166, 1999.
- Asakimori, K., Burnett, T.H., Cherry, M.L., et al. Cosmic ray composition and spectra: (1) Protons, in: Proc. 23rd Int. Cosmic Ray Conf., Calgary, vol. 2, pp. 21–24, 1993.
- Asakimori, K., Burnett, T.H., Cherry, M.L., et al. Cosmic-ray proton and helium spectra: results from the JACEE experiment. *Astrophys. J.* 502, 278–283, 1998.
- Beatty, J.J., Beach, S., Coutu, S., et al. Cosmic ray energetics and mass (CREAM): a detector for cosmic rays near the Knee, in: Proc. 26th Int. Cosmic Ray Conf., Salt Lake City, vol. 5, pp. 61–64, 1999.
- Beatty, J.J., Ahn, H.S., Allison, P.S., et al. Cosmic ray energetics and mass (CREAM) experiment timing charge detector, Astronomical telescopes and instrumentation, in: Angel, J.R.P., Breckinridge, J.B. (Eds.), Proc. SPIE Int. Symp. Optical Sci., Eng., and Instrum., vol. 4858, pp. 248–253, 2002.
- Biermann, P.L. Cosmic rays IV. The spectrum and chemical composition above  $10^4$  GeV. *Astron. Astrophys.* 271, 649–658, 1993.
- Gahbauer, F.H., Britton, J.W., Hermann, G., et al. A new detector for measurements of the composition of heavy cosmic ray nuclei beyond TeV-energies, in: Proc. 26th Int. Cosmic Ray Conf., Salt Lake City, vol. 5, pp. 25–28, 1999.
- Ganel, O., Seo, E.S., Ahn, H.S., et al. Cosmic ray energetics and mass: configuration and progress on construction and testing, in: Proc. 27th Int. Cosmic Ray Conf., Hamburg, vol. 6, pp. 2163–2166, 2001.
- Ganel, O., Seo, E.S., Ahn, H.S., et al. Cosmic ray energetics and mass (CREAM): calibrating a cosmic ray calorimeter, in: Proc. 10th Int. Conf. on Calorimetry in High Energy Physics, Pasadena, CA, pp. 133–138, 2002.
- Grigorov, N.L., Gubin, Y.V., Jakovlev, B.M., et al. Energy spectrum of primary cosmic rays in the  $10^{11}$  to  $10^{15}$  eV energy range according to the data of Proton-4 measurements, in: Proc. 12th Int. Cosmic Ray Conf., Tasmania, vol. 5, pp. 1746–1751, 1971.
- Koyama, M., Petre, R., Gotthelf, E.V., et al. Evidence for shock acceleration of high-energy electrons in the supernova remnant SN 1006. *Nature* 378, 255–258, 1995.
- Lagage, P.O., Cesarsky, C.J. Cosmic-ray shock acceleration in the presence of self-excited waves. *Astron. Astrophys.* 118, 223–228, 1983.
- Müller, D., Swordy, S.P., Meyer, P., et al. Energy spectra and composition of primary cosmic rays. *Astrophys. J.* 374, 356–365, 1991.
- Seo, E.S., Ahn, H.S., Beach, S., et al. Cosmic ray energetics and mass (CREAM) balloon experiment. *Adv. Space Res.* 30 (5), 1263–1272, 2002.
- Stuchlik, D., Black, R.K., Thompson, L.D. Results of the ultra-long duration balloon flight support system development. *Adv. Space Res.*, this issue, 2004, doi:10.1016/j.asr.2003.07.040.
- Wefel, J.P., Adams, J.H., Ahn, H.S., et al. The ATIC experiment: first balloon flight, in: Proc. 27th Int. Cosmic Ray Conf., Hamburg, vol. 6, pp. 2111–2113, 2001.